Research article

Exploring optical, electrochemical, thermal, and theoretical aspects of simple carbazole-derived organic dyes

Praveen Naik [a],[*], Nibedita Swain [a], R. Naik [b], Nainamalai Devarajan [c], Abdel-Basit Al-Odayni [d], Naaser A.Y. Abduh [e], Kavya S. Keremane [f], Devarajan Alagarasan [g], T. Aravinda [a], H.B. Shivaprasad [g]

[a] Department of Chemistry, Nitte Meenakshi Institute of Technology, Yelahanka, Bengaluru, 560064, Karnataka, India
[b] Department of Engineering and Materials Physics, Institute of Chemical Technology-Indian Oil Odisha Campus, Bhubaneswar, 751013, India
[c] Solid State and Structural Chemistry Unit, Indian Institute of Science, Bangalore, 560012, Karnataka, India
[d] Department of Restorative Dental Science, College of Dentistry, King Saud University, P. O. Box 60169, Riyadh, 11545, Saudi Arabia
[e] Department of Chemistry, College of Science, King Saud University, Saudi Arabia
[f] Materials Research Institute, The Pennsylvania State University, University Park, PA, 16802, USA
[g] Department of Physics, Nitte Meenakshi Institute of Technology, Yelahanka, Bengaluru, 560064, Karnataka, India

ARTICLE INFO

ABSTRACT

This study highlights the recent advancements in organic electronic materials and their potential for cost-effective optoelectronic devices. The investigation focuses on the molecular design, synthesis, and comprehensive analysis of two organic dyes, aiming to explore their suitability for optoelectronic applications. The dyes are strategically constructed with carbazole as the foundational structure, connecting two electron-withdrawing groups: barbituric acid (**Cz-BA**) and thiobarbituric acid (**Cz-TBA**). These dyes, featuring carbazole as the core and electron-withdrawing groups, demonstrate promising spectral, optical, electrochemical, thermal, and theoretical properties. They show strong potential for diverse optoelectronic applications, promising efficient light absorption and robust stability. The results endorse their suitability for practical optoelectronic systems.

1. Introduction

The organic semiconductor materials have attracted researchers across the globe owing to their possible application in optoelectronic devices such as organic light-emitting diodes (OLEDs), organic photovoltaics (OPVs), dye-sensitized solar cells (DSSCs), sensors, and photodetectors etc [1–8]. Organic materials display several advantages such as design versatility, good processability economical device, transparency, and tuneable optical and electrochemical properties, over their inorganic counterpart [9–12]. In recent years, electronic devices employing organic semiconductors have witnessed substantial advancement in terms of the lifetime, stability, and performance of the device [8]. Typically, the sensible molecular design of organic materials employed in the device architecture is the key to achieving ideal optoelectronics properties. A deep understanding of the correlation between the materials molecular structure and their properties is crucial for the development of advanced and efficient devices.

The integration of fused heteroaromatics like indole, carbazole, phenothiazine, and phenoxazine into a "push-pull" architecture has

---

* Corresponding author.
  E-mail address: praveennaik018@gmail.com (P. Naik).

emerged as a highly effective design strategy for creating organic materials with diverse optoelectronic applications [13–20]. Carbazole-based dyes, have garnered significant attention in various optoelectronics contexts, thanks to their remarkable attributes, including facile functionalization at multiple positions, straightforward synthesis, hole-transporting capabilities, and high molar extinction coefficients. These features have rendered carbazole and its derivatives as prominent building blocks for a wide array of optoelectronic devices, capitalizing on their distinctive optical and electrochemical properties [17,21–23]. Notably, the field of nonlinear optical (NLO) materials has also found carbazole-based compounds intriguing due to their distinctive electronic structure and donor-acceptor characteristics [24–28]. By integrating both electron-donating and electron-accepting groups into the carbazole framework, these compounds demonstrate enhanced charge transfer interactions, crucial for achieving efficient non-linear optical (NLO) responses. The electron-rich carbazole unit operates as a donor, facilitating electron transfer to electron-deficient acceptor groups. This molecular architecture not only enhances charge separation but also fosters intramolecular charge delocalization, culminating in superior nonlinear optical properties. As a result, the exploration of donor-acceptor systems built around carbazole holds immense potential for advanced NLO materials, customizable with tailored optical and electronic attributes, positioning them as promising candidates across photonics and optoelectronics [27–30,27–30,27–30]. The allure of carbazole and its derivatives further extends to their adaptability and distinctive traits, rendering them appealing for further exploration and development across various domains [31–37]. Current research endeavours concentrate on refining their electronic and optical features, alongside the creation of novel carbazole-based compounds, engineered to deliver enhanced performance and functionality for diverse applications.

The electron-deficient nature of barbituric acid and thiobarbituric acid has garnered significant attention in the realm of optoelectronic devices, due to their exceptional photophysical characteristics [38–40]. Barbituric acid exposed to exhibit high absorbance and emission in the ultraviolet (UV) range. Beyond their applications in solar cells, barbituric acid and thiobarbituric acid have been explored for their potential roles in OLEDs, serving as blue light emitting materials, and as photosensitizers in DSSCs [41–43]. Both barbituric acid and thiobarbituric acid have exhibited good electroluminescence properties, including high brightness and efficiency, and have shown promise as light emitting materials for OLEDs. Overall, the distinctive photophysical and electronic properties of barbituric acid and thiobarbituric acid render them compelling materials for diverse applications in the field of optoelectronics [41, 44].

Ongoing research is actively exploring the full potential of these materials in the field, encompassing the development of new derivatives and the optimization of device architectures. In this regard, we report simple carbazole based organic dyes carrying with two withdrawing groups i.e., barbituric acid and thiobarbituric acid. The synthesized dye's structure was validated through spectral analysis. To evaluate their suitability for potential optoelectronic applications, the synthesized dyes underwent thorough examination through photophysical and electrochemical studies. Additionally, the assessment was complemented by Density Functional Theory (DFT) calculations and Time-Dependent Density Functional Theory (TD-DFT) calculations.

2. Experimental section

2.1. Materials and methods

All materials and solvents were procured from commercial suppliers and utilized without further purification. The molecular structures of **Cz-BA** and **Cz-TBA** were conclusively confirmed using various analytical techniques, including NMR spectroscopy (Bruker 400 and 100 MHz), High-Resolution Mass Spectrometry (HRMS), and elemental analysis (Flash EA1112 CHN analyser). UV–Visible spectra and fluorescence emissions were recorded in tetrahydrofuran (THF) solution at room temperature using a UV–Visible and fluorescence spectrophotometer. Cyclic voltammetry (CV) measurements were performed with a three-electrode setup submerged in an acetonitrile solution containing a supporting electrolyte (0.1 M tetrabutylammonium hexafluorophosphate) at a scan rate of 0.1 V/s, employing a CHI400A electrochemical workstation. To ensure data reproducibility, five complete cycles were recorded. Furthermore, comprehensive DFT and TD-DFT calculations, along with MESP maps, were conducted at the B3LYP/6-31G* level using the BIOVIA Turbomole 2022 software package.

2.2. Synthesis

2.2.1. Synthesis of N-ethyl carbazole-6-oxothymine (Cz-BA)
0.25 g (0.001 mmol) of *N*-ethyl carbazole carboxaldehyde was taken in 10 ml of absolute methanol was stirred at 60 °C for 30 min. Subsequently, 0.5 g (0.003 mmol) of barbituric acid was gradually added with continuous stirring. The reaction mixture was then stirred for 10–12 h at 60 °C. Following the reaction's completion, the precipitated solid was filtered and rinsed with pre-cooled ethanol. The obtained dye underwent additional purification through recrystallization in a dichloromethane (DCM)/methanol mixture, yielding a pure yellow solid.

Yield 85 %, ^{1}H NMR (400 MHz, DMSO-d_6, ppm), 11.30 (s 1H), 11.19 (s 1H), 9.30 (d, 1H), 8.65 (dd, 1H), 8.54 (s, 1H), 8.20 (d, 1H), 7.75 (m, 2H), 7.57 (t, 1H), 7.34 (t, 1H), 4.53 (m, 2H), 1.38 (t, 3H). ^{13}C NMR (100 MHz, DMSO-d_6, ppm): 168.3, 164.8, 163.0, 157.4, 150.8, 143.2, 140.8, 133.9, 130.1, 127.3, 124.0, 123.0, 122.8, 121.1, 121.0, 114.6, 110.6, 109.6, 40.1, 40.0, 39.8, 14.3, CHN Analysis analytical calculated for $C_{19}H_{15}N_3O_3$: C - 68.46; H - 4.54; N - 12.61. found C - 68.43; H - 4.57; N - 12.59. Mass: HRMS 334.1192 [M+1].

2.2.2. Synthesis of N-ethyl carbazole-6-oxo thiothymine (Cz-TBA)
0.25 g (0.001 mmol) of N-ethyl carbazole carboxaldehyde was taken in 10 ml of methanol and stirred at 65 °C for 30 min. Subsequently, 0.5 g (0.003 mmol) of 2-thiobarbituric acid (was added to the clear solution, and stirring was continued for 10–12 h at a

constant temperature. The precipitated solid formed was collected, filtered, and washed with pre-cooled ethanol. Subsequently, the obtained residue underwent recrystallization, leading to the formation of a pure red solid.

Yield 92 %, ^{1}H NMR (400 MHz, ppm), 12.39 (s, 1H), 12.30 (s, 1H), 9.35 (d, 1H), 8.69 (dd, 1H), 8.55 (s, 1H), 8.21 (d, 1H), 7.76 (m, 2H), 7.56 (t, 1H), 7.36 (t, 1H), 4.53 (m, 2H), 1.38 (t, 3H). ^{13}C NMR (100 MHz, DMSO-d_6, ppm): 192.5, 178.7, 173.3, 163.1, 160.7, 158.5, 143.6, 140.9, 130.7, 128.8, 127.3, 124.2, 123.0, 122.9, 122.8, 121.4, 120.7, 114.6, 110.7, 110.4, 110.1, 109.8, 40.1, 40.0, 39.8, 14.3, 14. 2 CHN Analysis analytical calculated for $C_{19}H_{15}N_3O_2S$: C - 65.31; H - 4.33; N - 12.03. found C - 65.30; H - 4.36; N - 12.0 Mass: HRMS 350.0963 [M+1].

3. Results and discussion

3.1. Chemistry

The synthesis of **Cz-BA** and **Cz-TBA** dyes followed a straightforward Knoevenagel condensation reaction [45,46], as depicted in Scheme 1. In this synthetic pathway, N-ethyl carbazole carboxaldehyde underwent condensation with barbituric acid and thiobarbituric acid, yielding the targeted **Cz-BA** and **Cz-TBA** dyes, respectively. The synthesis protocol resulted in a substantial yield of the dyes, which were subsequently purified via recrystallization.

3.1.1. Electronic absorption and emission studies

Fig. 1 depicts the UV–Vis absorption profiles of the **Cz-BA** and **Cz-TBA** dyes, meticulously recorded in THF solvent at room temperature using a Labman UV–Vis absorption spectrophotometer. The pertinent spectral data extracted from these measurements are summarized in Table 1. As illustrated in Fig. 1, both **Cz-BA** and **Cz-TBA** dyes exhibit distinctive dual absorption bands. The absorption peaks observed at 343 nm (**Cz-BA**) and 351 nm (**Cz-TBA**) stem from π-π* electronic transitions originating within the donor component. The absorption signals manifesting at higher wavelengths, specifically at 441 nm (**Cz-BA**) and 473 nm (**Cz-TBA**), can be attributed to ICT (intramolecular charge transfer) phenomena, whereby, electron-deficient barbituric acid and thiobarbituric acid acceptor units engage in interactions with the carbazole donor moiety. Notably, the carbazole dye integrating thiobarbituric acid exhibits a noteworthy bathochromic (red) shift. Furthermore, the optical band gaps (E_{0-0}) of **Cz-BA** and **Cz-TBA** dyes were deduced from the normalized absorption spectrum, yielding values of 2.58 and 2.42 eV, individually. Moreover, the molar extinction coefficients (ε) for **Cz-BA** and **Cz-TBA** dyes were quantified as 26,543 $M^{-1}cm^{-1}$ and 36,490 $M^{-1}cm^{-1}$, respectively. These values underscore their remarkable light-absorbing capabilities and signify their potential for efficacious light absorption.

Fluorescence emission spectra of Cz-BA and Cz-TBA dyes were precisely recorded in THF solutions, corresponding to their respective excitation wavelengths. Illustrated in Fig. 2, the normalized emission spectra for both Cz-BA and Cz-TBA dyes in THF solution are displayed, with their corresponding spectral values summarized in Table 3. Singular, distinct emission bands were observed at 506 nm (Cz-BA) and 519 nm (Cz-TBA). In addition, their Stokes shift values were calculated using the UV–Vis absorption and fluorescence emission spectra. The computed values were found to be 65 nm for **Cz-BA** and 46 nm for **Cz-TBA**, as detailed in Table 1. The notably larger Stokes shift for **Cz-BA** in comparison to **Cz-TBA** underscores its effective intramolecular charge transfer (ICT) characteristics.

3.2. Thermal behaviour

The thermal characteristics and stability of the fluoranthene derivatives were comprehensively examined using TGA analysis. In particular, the decomposition temperature (T_d) of both **Cz-BA** and **Cz-TBA** dyes were accurately determined through TGA, and the resulting plots are graphically presented in Fig. 3. The experimental procedure involved subjecting the samples of **Cz-BA** and **Cz-TBA** dyes to controlled heating within an inert nitrogen gas atmosphere, with a gradual temperature increase rate of 10 °C per minute. The results indicate that the decomposition temperatures (T_d 5 %) corresponding to a 5 % weight loss were found to be 332 °C for **Cz-BA** and 310 °C for **Cz-TBA**, respectively. The notably high T_d values exhibited by these dyes hold significant implications, suggesting their suitability for applications requiring elevated temperature operations. This enhanced thermal stability underscores their potential for integration into device fabrication processes that demand resilience in the face of challenging thermal conditions.
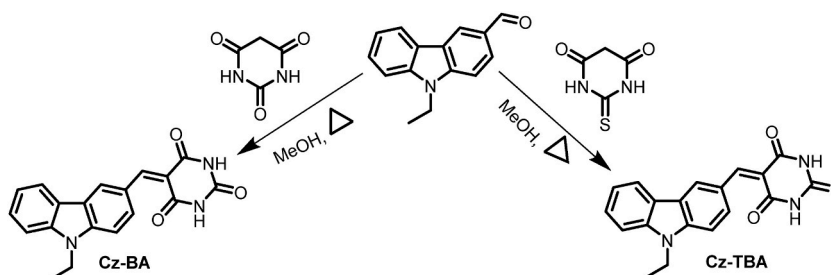
Scheme 1. Synthetic routes of the carbazole-based dyes, Cz-BA and Cz-TBA.

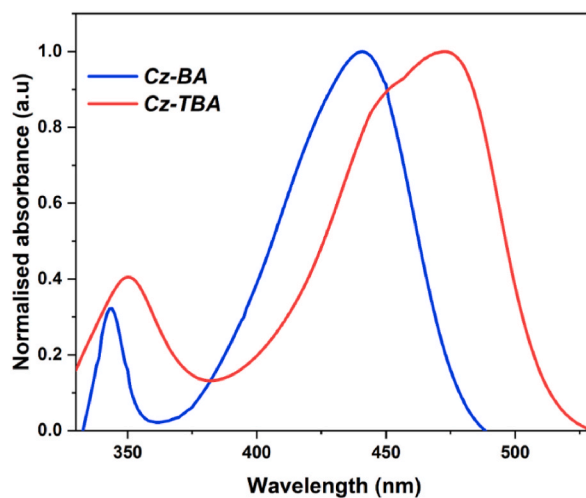**Fig. 1.** Normalized UV–Visible absorption spectra of **Cz-BA** and **Cz-TBA**.

Table 1
Optical properties of Cz-BA and Cz-TBA.

Dyes	Cz-BA	Cz-TBA
λ_{abs} (nm)	441	473
λ_{em} (nm)	506	519
ε	26,543 $M^{-1}cm^{-1}$	36,490 $M^{-1}cm^{-1}$
Stoke Shift (nm)	65	46
E_{0-0}, Optical (eV)	2.58	2.42

Table 2
Electronic parameters obtained from DFT calculations.

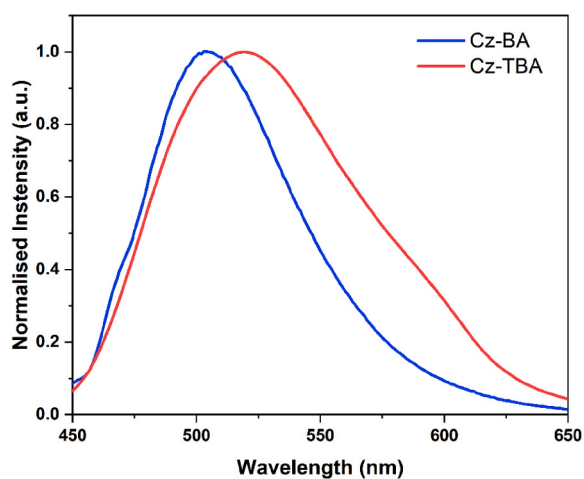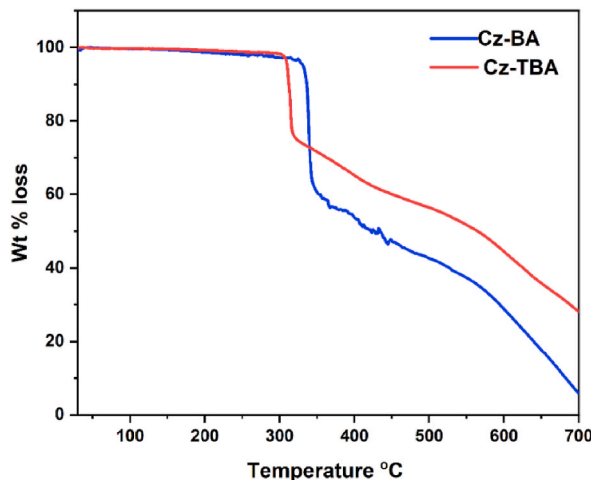| Dyes	Bandgap (eV)	HOMO (eV)	LUMO (eV)
Cz-BA	3.23	−5.63	−2.40
Cz-TBA	3.03	−5.68	−2.65

Fig. 2. Normalized fluorescence emission spectra of **Cz-BA** and **Cz-TBA**.

Table 3

Electronic absorption parameters obtained from TD-DFT calculations.

Dyes	λ_{abs}^I (nm)	λ_{abs}^S (nm)	f = OS^I	f = OS^S
Cz-BA	431	431	0.43	0.43
Cz-TBA	461	461	0.51	0.51

^{I} - isolate dye and ^{S} - Chloroform solvent.

Fig. 3. TGA analysis of **Cz-BA** and **Cz-TBA** dyes.

3.3. Computational studies

DFT calculations were executed to evaluate the electronic feasibility and characteristics of **Cz-BA** and **Cz-TBA** dyes, encompassing both ground and excited states, through the utilization of the Biovia Turbomole 2022 software package [47–49]. Employing the B3LYP/6-31G* level [50; 51], the electron density distribution in the HOMO and LUMO energy levels, along with the optimized geometries obtained from Turbomole, are visually represented in Figs. 4 and 5. Numerical values derived from these calculations are compiled in Table 2. Initially, molecular geometry optimization was conducted at the AM1 semiempirical level. The 3-D optimized structures distinctly portray efficient charge separation in the frontier molecular orbital energy levels. In the HOMO levels, the electron density predominantly localizes on the carbazole units for both dyes, showcasing their electron-rich donor nature. Conversely, in the LUMO levels, the electron clouds notably shift towards the acceptor unit, signifying their effective electron-accepting characteristics. Notably, the calculation underscores that the electron density of the LUMO energy levels in both the dyes has shifted towards the acceptor units.

In Fig. 6, ESP maps of **Cz-BA** and **Cz-TBA** offer a detailed view of the total charge density distribution at various spatial points surrounding the dye molecules. The alignment of cavity boundaries in the molecules with the density isosurface in the ESP plot visually represents the total charge distribution, encompassing electronegativity, dipole moment, and sites of chemical reactivity within the molecule. Distinct colors in the ESP plot correspond to electrostatic potential values, organized in the order of blue > green > yellow > orange > red. Following this color scheme, red and blue contours on the plot denote electron-rich and electron-deficient regions, respectively, indicating the presence of positive and negative charges on the cavity surface. This dynamic interplay establishes local electric fields within the cavity [52–54]. As a result, ESP plots serve as a vivid visualization of the movement of electron density from the donor species to the acceptor/anchoring unit through spacer units. This phenomenon significantly contributes to efficient electron
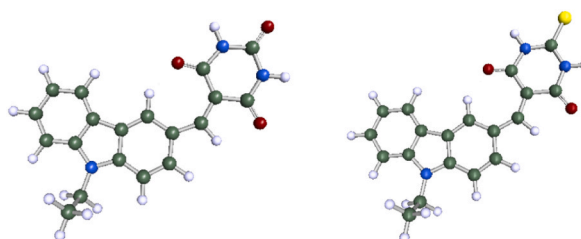
Fig. 4. Optimize the structure of the synthesized dyes **Cz-BA** and **Cz-TBA**.
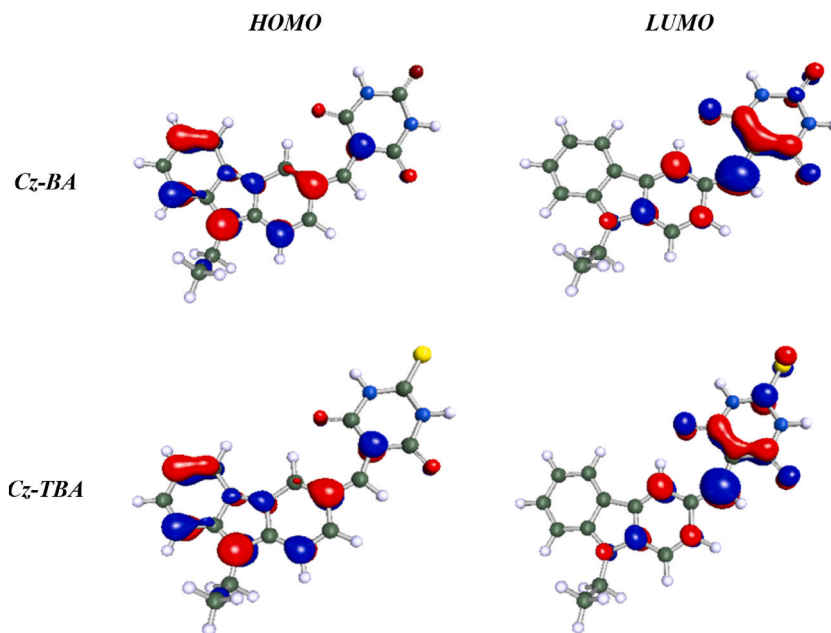
HOMO   LUMO

Cz-BA

Cz-TBA

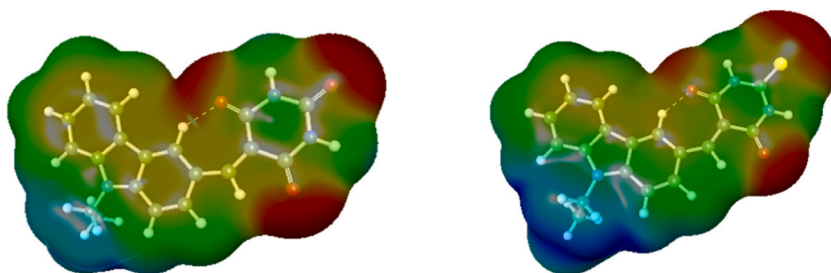**Fig. 5.** HOMO-LUMO energy levels of **Cz-BA and Cz-TBA**.

Fig. 6. ESP mapping on the iso density surface of Cz-**BA** and **Cz-TBA**.

transfer in both **Cz-BA** and **Cz-TBA**, as demonstrated by the distinctive patterns revealed in the ESP maps.

TD-DFT serves as a computational tool for comprehending the electronic behaviours of molecules [55,56,], elucidating light absorption in dyes like **Cz-BA** and **Cz-TBA** through absorption wavelengths (λ_{abs}) and oscillator strengths (f). This method simulates electronic transitions over time, aiding researchers in optimizing dyes for diverse applications based on their absorption traits. Fig. 7 portrays simulated absorption spectra of **Cz-BA** and **Cz-TBA**, stemming from B3LYP/6-31G* calculations in gaseous and THF solvent phases, detailed in Table 3. Oscillator strength (f) gauges the likelihood of electronic transitions, with higher values indicating higher probability. Remarkably, **Cz-BA** and **Cz-TBA** exhibit identical λ_{abs} and **f** for isolate (I) and solvent (S) phases, signifying consistent
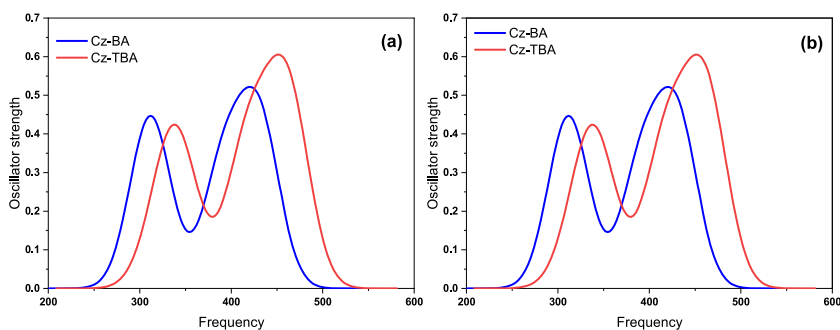
Fig. 7. Simulated electronic absorption of Cz-BA and Cz-TBA dyes in (a) gaseous state and (b) THF solvent.

absorption across environments. Fig. 7 further demonstrates two distinct peaks in simulated absorption spectra, correlating with π-π* transitions and ICT phenomena. This observation aligns harmoniously with UV–Vis absorption spectra derived from real-world data, validating the chosen basis set and XC functional. The incorporation of DFT and time-dependent perturbation theory in TD-DFT enables the computation and analysis of absorption properties. By comparing TD-DFT outcomes with experimental data, researchers refine models, gaining enhanced insights into dye electronic structures. This knowledge underpins tasks from developing purpose-specific dyes to tailoring properties for specific technological needs.

3.4. Organic electronics applications

3.4.1. Dyes as photosensitizers for DSSCs

The energy level diagram illustrated in Fig. 8, along with the comprehensive data provided in Table 4, encapsulates the calculated HOMO-LUMO values and E_{0-0} values for **Cz-BA** and **Cz-TBA** dyes. These values were derived from optical and cyclic voltammogram analyses, with Fig. S7 presenting corresponding cyclic voltammogram traces. This collective information serves as a crucial foundation for assessing the potential suitability of these organic dyes as photosensitizers in DSSC applications.

A noteworthy aspect is the positioning of the HOMO energy levels for these dyes, extending deeper than both the Nernst potential of the I_3^-/I^- electrolyte system and the conduction band (CB) of TiO2. This characteristic underscores their efficacy in facilitating the regeneration and reduction of the oxidized dye by the electrolyte species. Simultaneously, the estimated LUMO levels are favourably situated relative to the CB edge of TiO2, ensuring efficient processes of charge injection and dye regeneration. The oxidation potentials obtained from cyclic voltammetry studies were utilized to calculate their ESOP values using Equation (1).

$$HOMO = -[E^{OX} - E_{1/2}(ferrocene) + 4.8 \text{ eV }]. \tag{1}$$

Here, E^{OX} represents the reduction potential of dyes, and $E_{1/2}$ (ferrocene) is 0.17 eV. Additionally, their GSOP values were computed from the obtained E_{0-0} (optical band-gap) and ESOP values, as expressed in Equation (2):

$$LUMO = [HOMO - E_{0-0}] \text{ eV}. \tag{2}$$

To complement this analysis, we conducted calculations of essential thermodynamic parameters, including ΔGreg (Gibbs free energy for dye regeneration), ΔGinj (Gibbs free energy for electron injection), and ΔGrec (Gibbs free energy for charge recombination). Equations (3)–(5) were utilized for these calculations, considering Nernst potentials against the standard calomel electrode (SCE) for the CB edge of TiO2 and the I_3^-/I^- electrolyte system, which are −4.2 eV and −5.2 eV, respectively.

$$\Delta G_{inj} = E_{LUMO} - E_{CB} (TiO_2) \tag{3}$$

$$\Delta G_{reg} = E \left(I_3^- / I^\bullet \right) - E_{HOMO} \tag{4}$$

$$\Delta G_{rec} = E_{CB} (TiO_2) - E_{HOMO} \tag{5}$$

Table 4 summarizes the calculated values of these thermodynamic parameters for **Cz-BA** and **Cz-TBA** dyes, providing a concise overview of their performance in terms of ΔGinj, ΔGreg, and ΔGrec. Significantly, both the dyes exhibit favourable thermodynamic driving forces for charge injection and dye regeneration, meeting the specified range [57,58,]. This indicates promising potential for these dyes as sensitizers, as they meet the electrochemical prerequisites necessary for efficient charge transport in DSSC applications.

3.4.2. Refractive index calculation from E_{0-0} through various theoretical model

The optical bandgap and refractive index (n) stand as critical and fundamental parameters in assessing the suitability of any material. Theoretical relationships, particularly equations involving the refractive index and optical bandgap, provide insights into the optical and electronic characteristics of a material. In numerous cases, the refractive index exhibits an inverse relationship with the bandgap. The linear refractive index of **Cz-BA** and **Cz-TBA** can be determined using the well-known Dimitrov and Sakka relation [59].

$$\frac{n^2 - 1}{n^2 + 2} = 1 - \sqrt{\frac{E_{0-0}}{20}} \tag{6}$$

Here 'E_{0-0}' represents the optical bandgap. The computed refractive index values are detailed in Table 5. The high-frequency dielectric constant (ε_∞) is determined as n^2, utilizing the refractive index obtained from equation (1), and the results are provided in Table 5 [60].

Another approach to establishing a relationship between n and E_{0-0} was undertaken by Moss [60] relying on the material's energy levels. This relationship is expressed as, $E_{0-0} \times n^4 = k$ (constant). Rearranging the above equation,

$$n_M = \sqrt[4]{\frac{95}{E_{0-0}}} \tag{7}$$

In this equation, the constant k s assigned a value of 95 eV, where n represent the refractive index. This relationship is employed to calculate refractive loss, enhancing the solar cell's conversion parameter. Following this, Ravindra [61] proposed a modification to the aforementioned relation, presenting an alternative model that accounts for the constant difference between the average and optical
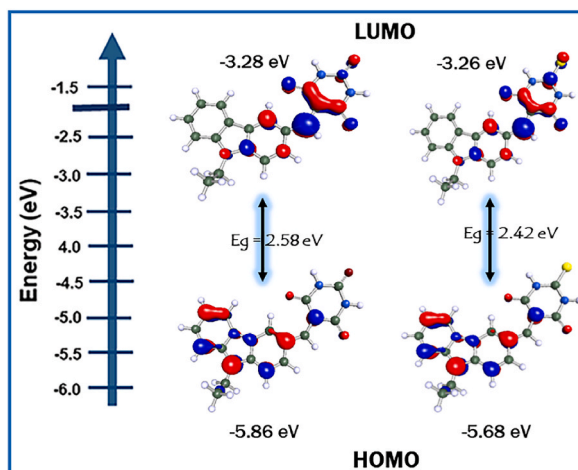
Fig. 8. Energy level diagram of **Cz-BA** and **Cz-TBA** dyes.

Table 4
Theoretical thermodynamics properties of Cz-BA and Cz-TBA dyes.

Dyes	E^{OX} (V)	HOMO (eV)	LUMO (eV)	ΔG_{inj} (eV)	ΔG_{reg} (eV)	ΔG_{rec} (eV)
Cz-BA	1.23	−5.86	−3.28	0.92	0.66	1.43
Cz-TBA	1.05	−5.68	−3.26	0.94	0.48	1.48

Table 5
Theoretical calculation of refractive index from models for Cz-BA and Cz-TBA dyes.

Dyes	Refractive index				
	$n_{[DS]}$	n_M	n_R	$n_{[HV]}$	n_T
Cz-BA	2.308	2.307	2.007	2.230	2.270
Cz-TBA	2.311	2.309	2.013	2.233	2.273

energy gaps. The relation is expressed as:

$$n_R = 4.084 - [0.62 \times E_{00}] \tag{8}$$

Moss confirmed the validity of this relation for bandgaps less than 4 eV; however, it may generate impractical values for extremely low and high optical energy values. Herve-Vandamme [62], relying on oscillator theory, introduced an alternative relation suitable for materials with low optical energy gaps:

$$n^2 = 1 + \left(\frac{A}{E_{00} + B}\right)^2 \tag{9}$$

Here, A is 13.6 eV, representing the ionization energy of hydrogen. The relation can be expressed as:

$$n_{[HV]} = \sqrt{1 + \left(\frac{13.6}{E_{00} + 3.47}\right)^2} \tag{10}$$

In addition to the aforementioned relations, Tripathy [63] proposed an exponentially decreasing relationship between n and E_{00} that characterizes the refractive index of materials in relation to their corresponding bandgaps:

$$n_T = 1.73 \times \left[1 + 1.9017 \times e^{-0.539 \times E_{00}}\right] \tag{11}$$

The theoretical values of 'n' are presented in Table 5. It is evident that the calculated 'n' values for **Cz-TBA** are higher than those for the **Cz-BA** material. This observation aligns with the inverse relationship between 'n' and E_{0-0}. As per Moss's rule, given that the bandgap of **Cz-BA** is greater than that of **Cz-TBA**, the refractive index of **Cz-BA** is consequently less than that of **Cz-TBA**.

3.4.3. Nonlinear optical parameters

Nonlinearity is a characteristic of a material that manifests its polarizability [64]. As the intensity of an electromagnetic wave

incident on the material increases, the material begins to exhibit nonlinear behaviour. As a result, the material's overall polarizability is affected by the electric field in various orders, and the connection between the electric field and polarization vector is articulated as [65].

$$P = \chi^{(1)}.E + P_{NL} \tag{12}$$

$$\text{or, } P = \left[\chi^{(1)}.E + \chi^{(2)}.E^2 + \chi^{(3)}.E^3 + \ldots\right]$$

Here $\chi^{(1)}$ represents the linear optical susceptibility, and $\chi^{(2)}$ and $\chi^{(3)}$ denote the second and third-order nonlinear susceptibilities, individually. The inclusion of the first and third-order terms in this expression offers valuable insights into the nonlinear behaviour exhibited by the material.

As per the Miller's empirical rule, the first nonlinear susceptibility ($\chi^{(1)}$) and third-order nonlinearity ($\chi^{(3)}$) can be computed using the following relations [66],

$$\chi^{(1)} = \frac{(n^2 - 1)}{4\pi}$$

$$\text{and } \chi^{(3)} = A\frac{(n^2 - 1)^4}{(4\pi)^4} = A\left(\chi^{(1)}\right)^4 \tag{13}$$

Here n_0 represents the static refractive index at $h\nu \to 0$ and $A = 1.7 \times 10^{-10}$ e.s.u. The computed nonlinear susceptibilities for the material are presented in Table 6.

Nonlinear refractive index ($\mathbf{n_2}$)

The nonlinear refractive index (n_2) of **Cz-BA** and **Cz-TBA** samples can be determined utilizing the modified Miller rule proposed by Tichy and Ticha [67]. The empirical relation provides an expression from which the nonlinear refractive index can be deduced, as follows:

$$n_2 = \frac{12\pi\chi^{(3)}}{n} \tag{14}$$

The estimated values of n_2 for **Cz-BA** and **Cz-TBA** is tabulated in Table 6.

4. Conclusion

In conclusion, our investigation of carbazole-based dyes, **Cz-BA** and **Cz-TBA**, has unveiled their promising potential for diverse optoelectronic applications, with a particular emphasis on their suitability for DSSC and NLO applications. Through a combination of comprehensive spectral and theoretical analyses, we have shed light on their optical properties, including refractive index calculations and nonlinear optical parameters like the nonlinear refractive index (n_2), positioning them as promising candidates for nonlinear optical applications. Furthermore, our photophysical studies have underscored their effective light-absorption and emission behaviour, while DFT and TD-DFT simulations have provided robust validation of their electronic characteristics and absorption spectra in congruence with experimental data. The successful design and characterization of these dyes represent a significant leap forward in the practical utilization of advanced organic materials for DSSCs, making substantial contributions to materials science while offering innovative solutions for a wide range of real-world optoelectronic challenges. This marks a significant stride in the practical application of these advanced organic materials in the renewable energy sector.

CRediT authorship contribution statement

Praveen Naik: Writing – original draft, Writing – review & editing, Visualization, Validation, Supervision, Software, Resources, Methodology, Investigation, Formal analysis, Conceptualization. **Nibedita Swain:** Validation, Resources, Methodology, Investigation, Formal analysis, Data curation. **R. Naik:** Resources, Methodology, Investigation, Formal analysis, Data curation. **Nainamalai Devarajan:** Resources, Methodology, Investigation. **Abdel-Basit Al-Odayni:** Resources, Funding acquisition. **Naaser A.Y. Abduh:** Resources. **Kavya S. Keremane:** Writing – review & editing, Validation, Resources. **Devarajan Alagarasan:** Investigation, Formal analysis. **T. Aravinda:** Resources. **H.B. Shivaprasad:** Resources.

Table 6
Theoretical calculation of refractive index from models for Cz-BA and Cz-TBA samples.

Parameters	ε_∞	$\chi^{(1)}$	$\chi^{(3)}$	n_2
Cz-TB	5.330	0.344	2.401×10^{-12}	3.919×10^{-11}
Cz-TBA	5.341	0.345	2.426×10^{-12}	3.955×10^{-11}

Declaration of competing interest

The authors declare the following financial interests/personal relationships which may be considered as potential competing interests:

Authors declare no conflict of interest If there are other authors, they declare that they have no known competing financial interests or personal relationships that could have appeared to influence the work reported in this paper.

Acknowledgments

Appendix A. Supplementary data

Supplementary data to this article can be found online at https://doi.org/10.1016/j.heliyon.2024.e25624.

References

[1] Y. Gong, S. Zhang, H. Gao, Z. Ma, S. Hu, Z. Tan, Recent advances and comprehensive insights on nickel oxide in emerging optoelectronic devices, Sustain. Energy Fuels 4 (2020) 4415–4458, https://doi.org/10.1039/D0SE00621A.

[2] S. Manzhos, C.C. Chueh, G. Giorgi, T. Kubo, G. Saianand, J. Lüder, P. Sonar, M. Ihara, Materials design and optimization for next-generation solar cell and light-emitting technologies, J. Phys. Chem. Lett. 12 (2021) 4638–4657, doi:10.1021/acs.jpclett.1c00714.

[3] L. Ji, J. Shi, J. Wei, T. Yu, W. Huang, Air-stable organic radicals: new-generation materials for Flexible electronics? Adv. Mater. 32 (2020) 1908015, https://doi.org/10.1002/adma.201908015.

[4] Q. Lu, Z. Yang, X. Meng, Y. Yue, M.A. Ahmad, W. Zhang, S. Zhang, Y. Zhang, Z. Liu, W. Chen, A review on encapsulation Technology from organic light emitting diodes to organic and perovskite solar cells, Adv. Funct. Mater. 31 (2021) 2100151, https://doi.org/10.1002/adfm.202100151.

[5] M. Yahya, A. Bouziani, C. Ocak, Z. Seferoğlu, M. Sillanpää, Organic/metal-organic photosensitizers for dye-sensitized solar cells (DSSC): recent developments, new trends, and future perceptions, Dyes Pigments 192 (2021) 109227, https://doi.org/10.1016/j.dyepig.2021.109227.

[6] D. Yang, D. Ma, Development of organic semiconductor photodetectors: from mechanism to applications, Adv. Opt. Mater. 7 (2019) 1800522, https://doi.org/10.1002/adom.201800522.

[7] S. Lee, H. Kim, Y. Kim, Progress in organic semiconducting materials with high thermal stability for organic light-emitting devices, InfoMat 3 (2021) 61–81, https://doi.org/10.1002/inf2.12123.

[8] S. Revoju, A. Matuhina, L. Canil, H. Salonen, A. Hiltunen, A. Abate, P. Vivo, Structure-induced optoelectronic properties of phenothiazine-based materials, J Mater Chem C Mater 8 (2020) 15486–15506, https://doi.org/10.1039/D0TC03421E.

[9] P.C.Y. Chow, T. Someya, Organic photodetectors for next-generation wearable electronics, Adv. Mater. 32 (2020) 1902045, https://doi.org/10.1002/adma.201902045.

[10] M. Kim, S.U. Ryu, S.A. Park, K. Choi, T. Kim, D. Chung, T. Park, Donor–acceptor-Conjugated polymer for high-performance organic field-effect transistors: a progress report, Adv. Funct. Mater. 30 (2020) 1904545, https://doi.org/10.1002/adfm.201904545.

[11] Cheng P., Li G., Zhan X., Yang Y., Next-generation organic photovoltaics based on non-fullerene acceptors, Nature Photonics 12 (2018) 131–142, doi.org/10.1038/s41566-018-0104-9.

[12] J. Miao, F. Zhang, Recent progress on highly sensitive perovskite photodetectors, J Mater Chem C 7 (2019) 1741–1791, https://doi.org/10.1039/C8TC06089D.

[13] N. Odedara, N. Borane, R. Patel, R. Boddula, A review on the milestones of blue light-emitting materials in India, Organic Materials 5 (2023) 1–20, https://doi.org/10.1055/S-0042-1757980.

[14] F. Grifoni, M. Bonomo, W. Naim, N. Barbero, T. Alnasser, I. Dzeba, M. Giordano, A. Tsaturyan, M. Urbani, T. Torres, C. Barolo, F. Sauvage, Toward sustainable, colorless, and transparent photovoltaics: state of the art and perspectives for the development of selective near-infrared dye-sensitized solar cells, Adv. Energy Mater. 11 (2021) 2101598, https://doi.org/10.1002/aenm.202101598.

[15] N. Pilicode, N.K. M, M. Acharya, P. Naik, S.M. N, A.V. Adhikari, New blue light emitting cyanopyridine based conjugated polymers: from molecular engineering to PLED applications, J. Photochem. Photobiol. Chem. 378 (2019) 38–45, https://doi.org/10.1016/j.jphotochem.2019.04.012.

[16] N. Pilicode, P. Naik, K.M. Nimith, M. Acharya, M.N. Satyanarayan, A.V. Adhikari, New cyanopyridine-based π-conjugative poly(azomethine)s: synthesis, characterization and electroluminescence studies, Polym. Adv. Technol. 32 (2021) 131–141, https://doi.org/10.1002/pat.5067.

[17] P. Naik, R. Su, M.R. Elmorsy, A. El-Shafei, A.V. Adhikari, Investigation of new carbazole based metal-free dyes as active photo-sensitizers/co-sensitizers for DSSCs, Dyes Pigments 149 (2018) 177–187, https://doi.org/10.1016/J.DYEPIG.2017.09.068.

[18] P. Naik, R. Su, M.R. Elmorsy, D.D. Babu, A. El-shafei, Adhikari A.V., Molecular design and theoretical investigation of new metal-free heteroaromatic dyes with D- p -A architecture as photosensitizers for DSSC application, J. Photochem. Photobiol. Chem. 345 (2017) 63–73, https://doi.org/10.1016/j.jphotochem.2017.05.033.

[19] P. Naik, R. Su, M.R. Elmorsy, A. El-Shafei, A.V. Adhikari, New carbazole based dyes as effective co-sensitizers for DSSCs sensitized with ruthenium (II) complex (NCSU-10), J. Energy Chem. 27 (2018) 351–360, https://doi.org/10.1016/J.JECHEM.2017.12.013.

[20] Naik P., Elmorsy M.R., Su R., Babu D.D., El-shafei A., Adhikari A.V., New carbazole based metal-free organic dyes with D-π-A-π-A architecture for DSSCs: Synthesis, theoretical and cell performance studies. Sol. Energy, 153 (2017) 600 - 610, doi.org/10.1016/j.solener.2017.05.088.

[21] G. Bubniene, T. Malinauskas, M. Daskeviciene, V. Jankauskas, V. Getautis, Easily functionalizable carbazole based building blocks with extended conjugated systems for optoelectronic applications, Tetrahedron 66 (2010) 3199–3206, https://doi.org/10.1016/j.tet.2010.02.086.

[22] H.Y. Wang, F. Liu, L.H. Xie, C. Tang, B. Peng, W. Huang, W. Wei, Topological arrangement of fluorenyl-substituted carbazole triads and starbursts: synthesis and optoelectronic properties, J. Phys. Chem. C 115 (2011) 6961–6967, doi:10.1021/jp200433e..

[23] Venkateswararao A., Thomas K.R.J., Lee C.P., Ho K.C., Synthesis and characterization of organic dyes containing 2,7-disubstituted carbazole π-linker, Tetrahedron Lett. 54 (2013) 3985–3989, doi.org/10.1016/j.tetlet.2013.05.069.

[24] K.R. Yoon, N.M. Byun, H. Lee, Synthesis and characterization of carbazole-based nonlinear optical polymers possessing chromophores in the main or side chains, Synth. Met. 157 (2007) 603–610, https://doi.org/10.1016/j.synthmet.2007.04.017.

[25] S. Xu, C. Fang, Y. Wu, W. Wu, Q. Guo, J. Zeng, X. Wang, Y. Liu, S. Cao, Photorefractive hyper-structured molecular glasses constructed by calix[4]resorcinarene core and carbazole-based methine nonlinear optical chromophore, Dyes Pigments 142 (2017) 8–16, https://doi.org/10.1016/J.DYEPIG.2017.03.001.

[26] S.J. Weishäupl, D.C. Mayer, E. Thyrhaug, J. Hauer, A. Pöthig, R.A. Fischer, A nitrophenyl-carbazole based push-pull linker as a building block for non-linear optical active coordination polymers: a structural and photophysical study, Dyes Pigments 186 (2021) 109012, https://doi.org/10.1016/J.DYEPIG.2020.109012.

[27] M. Khalid, M.U. Khan, I. Shafiq, R. Hussain, K. Mahmood, A. Hussain, R. Jawaria, A. Hussain, M. Imran, M.A. Assiri, A. Ali, M.F. ur Rehman, K. Sun, Y. Li, NLO potential exploration for D–π–A heterocyclic organic compounds by incorporation of various π-linkers and acceptor units, Arab. J. Chem. 14 (2021) 103295, https://doi.org/10.1016/J.ARABJC.2021.103295.

[28] Bodapati R., Dey G.R., Ramteke G.R., Krishnakanth K.N., Rao S.V., Jose K.V.J., Das S.K., Carbazole-based π-conjugated 2,2'-Bipyridines, a new class of organic chromophores: photophysical, ultrafast nonlinear optical and computational studies, Dyes Pigments 185 (2021) 108932, oi.org/10.1016/j.dyepig.2020.108932.

[29] S. Semin, X. Li, Y. Duan, T. Rasing, Nonlinear optical properties and applications of fluorenone molecular materials, Adv. Opt. Mater. 9 (2021) 2100327, https://doi.org/10.1002/ADOM.202100327.

[30] M.J. Cho, D.H. Choi, P.A. Sullivan, A.J.P. Akelaitis, L.R. Dalton, Recent progress in second-order nonlinear optical polymers and dendrimers, Prog. Polym. Sci. 33 (2008) 1013–1058, https://doi.org/10.1016/J.PROGPOLYMSCI.2008.07.007.

[31] S. Wang, H. Li, H. Huang, X. Cao, X. Chen, D. Cao, Porous organic polymers as a platform for sensing applications, Chem. Soc. Rev. 51 (2022) 2031–2080, https://doi.org/10.1039/D2CS00059H.

[32] M. Mahato, Y. Murakami, S.K. Das, Recent advances and applications of ionic liquids-based photonic materials, Appl. Mater. Today 32 (2023) 101808, https://doi.org/10.1016/J.APMT.2023.101808.

[33] F. Fang, L. Zhu, M. Li, Y. Song, M. Sun, D. Zhao, J. Zhang, Thermally activated delayed fluorescence material: an emerging class of metal-free luminophores for biomedical applications, Adv. Sci. 8 (2021) 2102970, https://doi.org/10.1002/ADVS.202102970.

[34] V. Nayana, B. Kandasubramanian, Polycarbazole and its derivatives: progress, synthesis, and applications, J. Polym. Res. 27 (9 27) (2020) 1–24, https://doi.org/10.1007/S10965-020-02254-7, 2020.

[35] H. Sun, F. Chen, Z.K. Chen, Recent progress on non-fullerene acceptors for organic photovoltaics, Mater. Today 24 (2019) 94–118, https://doi.org/10.1016/J.MATTOD.2018.09.004.

[36] Azzaroni O., Polymer brushes here, there, and everywhere: recent advances in their practical applications and emerging opportunities in multiple research fields, J. Polym. Sci. Polym. Chem. 50 (2012) 3225–3258, doi.org/10.1002/pola.26119.

[37] P. Naik, R. Su, A. El-Shafei, A.V. Adhikari, Improved photovoltaic performances of Ru (II) complex sensitized DSSCs by co-sensitization of carbazole based chromophores, Inorg. Chem. Commun. 86 (2017) 241–245, https://doi.org/10.1016/J.INOCHE.2017.10.030.

[38] P. Naik, D.D. Babu, G.K. Jayaprakash, A computational approach for screening carbazole based organic dyes as potential photosensitizers for DSSCs application, Results Chem 6 (2023) 101000, https://doi.org/10.1016/J.RECHEM.2023.101000.

[39] D.L. Obydennov, A.E. Simbirtseva, A.S. Shirinkin, M.Y. Kornev, V.Y. Sosnovskikh, A novel strategy for the functionalization and design of 4-methylene-4H-pyran merocyanines via enamination and 1,8-conjugate addition, Org. Biomol. Chem. 21 (2023) 600–620, https://doi.org/10.1039/D2OB01862D.

[40] B. Hosseinzadeh, A. Salimi Beni, A. Najafi Chermahini, R. Ghahary, A. Teimouri, Novel organic dyes with anchoring group of barbituric/thiobarbituric acid and their application in dye-sensitized solar cells, Synth. Met. 209 (2015) 1–10, https://doi.org/10.1016/J.SYNTHMET.2015.06.018.

[41] Shu Y., Mikosch A., Winzenberg K.N., Kemppinen P., Easton C.D., Bilic A., Forsyth C.M., Dunn C.J., Singh ThB., Collis G.E., N-Alkyl functionalized barbituric and thiobarbituric acid bithiophene derivatives for vacuum deposited n-channel OFETs, J Mater Chem C Mater 2 (2014) 3895, doi.org/10.1039/C4TC00002A.

[42] Babu D.D., Naik P., Keremane K.S., A simple D-A- π -A configured carbazole based dye as an active photo-sensitizer : a comparative investigation on different parameters of cell, J. Mol. Liq. 310 (2020) 113189, doi.org/10.1016/j.molliq.2020.113189.

[43] K.S. Keremane, I.M. Abdellah, P. Naik, A. El-Shafei, A.V. Adhikari, Simple thiophene-bridged D-π-A type chromophores for DSSCs: a comprehensive study of their sensitization and co-sensitization properties, Phys. Chem. Chem. Phys. 22 (2020) 23169–23184, https://doi.org/10.1039/D0CP02781B.

[44] P. Naik, M. Acharaya, N. Pilicode, A. El-Shafei, A.V. Adhikari, An Efficient Aniline-Based Co-Sensitizer for High Performance N3-Sensitized Solar Cells, ChemistrySelect 3 (2018) 12297–12302, https://doi.org/10.1002/slct.201802232.

[45] P. Naik, K.S. Keremane, M.R. Elmorsy, R. Su, A. El-Shafei, A.V. Adhikari, Highly efficient carbazole based co-sensitizers carrying electron deficient barbituric acid for NCSU-10 sensitized DSSCs, Sol. Energy 169 (2018) 386–391, https://doi.org/10.1016/J.SOLENER.2018.05.024.

[46] Kala V., Vineetha P.K., Manoj N., A simple cost effective carbazole–thiobarbituric acid conjugate as a ratiometric fluorescent probe for detection of mercury(II) ions in aqueous medium, New J. Chem. 41 (2017) 5176–5181, doi.org/10.1039/C7NJ00805H.

[47] P. Naik, A. Planchat, Y. Pellegrin, F. Odobel, A. Vasudeva Adhikari, Exploring the application of new carbazole based dyes as effective p-type photosensitizers in dye-sensitized solar cells, Sol. Energy 157 (2017) 1064–1073, https://doi.org/10.1016/j.solener.2017.09.024.

[48] N. Pilicode, P. Naik, A.V. Adhikari, Nicotinonitrile centered luminescent polymeric materials: structural, optical, electrochemical, and theoretical investigations, Polym. Eng. Sci. 60 (2020) 2550–2559, https://doi.org/10.1002/pen.25493.

[49] N. Pilicode, P. Naik, K.M. Nimith, M. Acharya, M.N. Satyanarayan, A.V. Adhikari, New cyanopyridine based conjugated polymers carrying auxiliary electron donors: from molecular design to blue emissive PLEDs, Dyes Pigments 174 (2020) 108046, https://doi.org/10.1016/j.dyepig.2019.108046.

[50] A. Azaid, M. Alaqarbeh, T. Abram, M. Raftani, R. Kacimi, Y. Khaddam, A. Sbai, T. Lakhlifi, M. Bouachrine, D-π-A push-pull chromophores based on N,N-Diethylaniline as a donor for NLO applications: effects of structural modification of π-linkers, J. Mol. Struct. 1295 (2024) 136602, https://doi.org/10.1016/J.MOLSTRUC.2023.136602.

[51] R. Kacimi, M. Raftani, T. Abram, A. Azaid, H. Ziyat, L. Bejjit, M.N. Bennani, M. Bouachrine, Theoretical design of D-π-A system new dyes candidate for DSSC application, Heliyon 7 (2021) e07171, https://doi.org/10.1016/j.heliyon.2021.e07171.

[52] P.K.M. Lokhande, K.K. Sonigara, M.M. Jadhav, D.S. Patil, S.S. Soni, N. Sekar, Multi-dentate carbazole based schiff base dyes with chlorovinylene group in spacer for dye-sensitized solar cells: a combined theoretical and experimental study, ChemistrySelect 4 (2019) 4044–4056, https://doi.org/10.1002/SLCT.201803940.

[53] P. Naik, N. Pilicode, K.S. Keremane, M. Acharya, A.V. Adhikari, Synthesis, optical, electrochemical, and computational investigation of new cyanopyridine-centered organic dyads, Opt. Mater. 142 (2023) 114002, https://doi.org/10.1016/J.OPTMAT.2023.114002.

[54] A. Mahmood, J.Y. Hu, B. Xiao, A. Tang, X. Wang, E. Zhou, Recent progress in porphyrin-based materials for organic solar cells, J Mater Chem A Mater 6 (2018) 16769–16797, https://doi.org/10.1039/C8TA06392C.

[55] A. Azaid, R. Kacimi, M. Alaqarbeh, M. Raftani, T. Abram, A. Sbai, T. Lakhlifi, M. Bouachrine, Design of a D–di–π–A architecture with different auxiliary donors for dye-sensitized solar cells: density functional theory/time-dependent-density functional theory study of the effect of secondary donors, Adv Theory Simul 6 (2023) 2300054, https://doi.org/10.1002/adts.202300054.

[56] Bourass M., Touimi Benjelloun A., Benzakour M., McHarfi M., Jhilal F., Hamidi M., Bouachrine M., The optoelectronic properties of organic materials based on triphenylamine that are relevant to organic solar photovoltaic cells, New J. Chem. 41 (2017) 13336–13346, doi.org/10.1039/C7NJ03272B.

[57] Oskam G., Bergeron B.V., Meyer G.J., Searson P.C., Pseudohalogens for dye-sensitized TiO₂ photoelectrochemical cells, J. Phys. Chem. B 105 (2001) 6867–6873, doi.org/10.1021/jp004411d.

[58] P. Qu, G.J. Meyer, Proton-controlled electron injection from molecular excited states to the empty states in nanocrystalline TiO₂, Langmuir 17 (2001) 6720–6728, https://doi.org/10.1021/la010939d.

[59] S.A. Mulenko, V.I. Rudenko, V.R. Liakhovetskyi, A.M. Brodin, N. Stefan, Large third-order optical nonlinearities in iron oxide thin films synthesized by reactive pulsed laser deposition, Opt. Mater. 60 (2016) 123–127, https://doi.org/10.1016/J.OPTMAT.2016.07.017.

[60] T.S. Moss, A relationship between the refractive index and the infra-red threshold of sensitivity for photoconductors, Proc. Phys. Soc. B 63 (1950) 167, https://doi.org/10.1088/0370-1301/63/3/302.

[61] N.M. Ravindra, S. Auluck, V.K. Srivastava, On the penn gap in semiconductors, Phys. Status Solidi 93 (1979), https://doi.org/10.1002/PSSB.2220930257. K155–K160.

[62] P. Hervé, L.K.J. Vandamme, General relation between refractive index and energy gap in semiconductors, Infrared Phys. Technol. 35 (1994) 609–615, https://doi.org/10.1016/1350-4495(94)90026-4.

[63] S.K. Tripathy, Refractive indices of semiconductors from energy gaps, Opt. Mater. 46 (2015) 240–246, https://doi.org/10.1016/J.OPTMAT.2015.04.026.

[64] Frenette M., Hatamimoslehabadi M., Bellinger-Buckley S., Laoui S., Bag S., Dantiste O., Rochford J., Yelleswarapu C., Nonlinear optical properties of multipyrrole dyes, Chem. Phys. Lett. 608 (2014) 303–307, doi.org/10.1016/j.cplett.2014.06.002.

[65] Frumar M., Frumarova B., Wagner T., Sujan G.K., Amorphous and Glassy Semiconducting Chalcogenides, Reference Module in Materials Science and Materials Engineering.Elsevier, (2016) doi.org/10.1016/B978-0-12-803581-8.09804-0.

[66] J.J. Wynne, Nonlinear optical spectroscopy of X(3) in LiNb03, Phys. Rev. Lett. 29 (1972) 650, https://doi.org/10.1103/PhysRevLett.29.650.

[67] H. Tichá, L. Tichý, Semiempirical relation between non-linear susceptibility (refractive index), linear refractive index and optical gap and its application to amorphous chalcogenides, J. Optoelectron. Adv. Mater. 4 (2002) 381–386.